Article

TRANSPARENT PROCESS

EMBO reports

Zebrafish facial lymphatics develop through sequential addition of venous and non-venous progenitors

Tiffany CY Eng[1], Wenxuan Chen[1], Kazuhide S Okuda[1,2], June P Misa[1], Yvonne Padberg[3,4], Kathryn E Crosier[1], Philip S Crosier[1], Christopher J Hall[1], Stefan Schulte-Merker[3,4], Benjamin M Hogan[2] & Jonathan W Astin[1,*]

Abstract

Lymphatic vessels are known to be derived from veins; however, recent lineage-tracing experiments propose that specific lymphatic networks may originate from both venous and non-venous sources. Despite this, direct evidence of a non-venous lymphatic progenitor is missing. Here, we show that the zebrafish facial lymphatic network is derived from three distinct progenitor populations that add sequentially to the developing facial lymphatic through a relay-like mechanism. We show that while two facial lymphatic progenitor populations are venous in origin, the third population, termed the ventral aorta lymphangioblast (VA-L), does not sprout from a vessel; instead, it arises from a migratory angioblast cell near the ventral aorta that initially lacks both venous and lymphatic markers, and contributes to the facial lymphatics and the hypobranchial artery. We propose that sequential addition of venous and non-venous progenitors allows the facial lymphatics to form in an area that is relatively devoid of veins. Overall, this study provides conclusive, live imaging-based evidence of a non-venous lymphatic progenitor and demonstrates that the origin and development of lymphatic vessels is context-dependent.

Keywords angioblast; lymphangiogenesis; lymphatic origin; lymphatic specification; Vegfr3 signalling

Subject Categories Development & Differentiation; Vascular Biology & Angiogenesis

DOI 10.15252/embr.201847079 | Received 14 September 2018 | Revised 30 January 2019 | Accepted 12 February 2019 | Published online 15 March 2019

EMBO Reports (2019) 20: e47079

Introduction

Lymphatic vessel development begins through a step-wise process wherein lymphatic progenitors are specified, migrate and then coalesce to form nascent lymphatic vessels. Prospero-related homeodomain transcription factor (PROX)1 is the master regulator of lymphatic endothelial cell (LEC) fate and is necessary for lymphatic progenitor specification in mammals [1,2]. Following specification, lymphatic progenitors sprout from the veins by vascular endothelial growth factor receptor (VEGFR)-3 signalling through its ligand, vascular endothelial growth factor (VEGF)-C [3–5]. While various models of venous lymphatic sprouting have been proposed, including the "ballooning" mechanism, whereby lymphangioblasts (migratory lymphatic progenitor cells) collectively sprout as several small sacs [6], and the "budding" mechanism where lymphangioblasts bud off as loosely interconnected cells [5,7], the exact mechanism by which lymphangioblasts coalesce into mature lymphatic vessels remains unclear.

Although veins are currently thought to be the predominant source of lymphatics, historically there have been two opposing models describing the origin of lymphatic progenitors. The first model, proposed by Florence Sabin, suggested that lymphatics sprout from the pre-existing venous endothelium [8], while the model proposed by Huntington and McClure suggested that perivascular lymphangioblasts in the mesenchyme fuse to form isolated lymphatic vessels that later establish a connection to the venous system [9,10]. Lineage-tracing experiments, particularly in mice and zebrafish, have largely supported Sabin's model, and until recently, veins were considered the sole contributor of the lymphatic vasculature in fish and mammals [11,12]. However, there is also evidence for a hybrid of these two models, wherein both venous and non-venous cells provide lymphatic progenitors. This "dual origin" model for lymphatics was first conceived 85 years ago when the anterior lymph sacs of the sea turtle were observed to have both a venous and mesenchymal origin [13], and this model is now supported by contemporary experiments in chick [14,15] and *Xenopus* [16]. Furthermore, recent lineage-tracing studies in mice have suggested that part of the cardiac, dermal and mesenteric lymphatic networks are formed by independent lymphangioblast clusters that

1 Department of Molecular Medicine & Pathology, School of Medical Sciences, The University of Auckland, Auckland, New Zealand
2 Division of Genomics of Development and Disease, Institute for Molecular Bioscience, The University of Queensland, Brisbane, QLD, Australia
3 Institute for Cardiovascular Organogenesis and Regeneration, Faculty of Medicine, WWU Münster, Münster, Germany
4 CiM Cluster of Excellence (EXC 1003-CiM), WWU Münster, Münster, Germany
*Corresponding author. Tel: +64 9 923 4480; E-mail: j.astin@auckland.ac.nz

appear to be non-venous in origin [17–19]. However, much of the recent evidence for non-venous lymphatic progenitors comes from genetic lineage tracing using Cre-LoxP recombination. As such, these results rely on complete Cre-mediated recombination and lineage-specific Cre activity [20,21]. Limitations in this technique have resulted in contradictory data regarding the vascular origin of non-venous progenitors in both the mouse dermal [19,22] and cardiac lymphatics [17,20]. Taken together, these various studies provide sometimes contradictory evidence that differentiated veins may not be the only progenitor source contributing to lymphatic development and direct evidence of a non-venous lymphatic progenitor still remains elusive.

The zebrafish has proven to be an invaluable tool for understanding lymphatic development, as their transparent embryos allow for high-resolution, *in vivo* live imaging of developing lymphatic vessels [11,23]. Similar to mammals, venous-derived lymphatic progenitors in zebrafish can be identified through Prox1 expression [24,25] and lymphatic sprouting is dependent on Vegfr3 (known as Flt4 in zebrafish) signalling [26–28]. There are also some discrepancies between the two animal models; for example, Vegfr3 signalling is required for lymphatic specification, via Prox1 induction, in the zebrafish trunk [25,29], despite having no effect on initial lymphatic specification in mice [3,5,30,31]. However, there still exists a relationship between VEGFR-3 and PROX1 in mammals, as the two interact via a positive feedback loop in order to maintain the lymphatic identity of LECs [31]. Interestingly, a recent study has suggested that, similar to mammals, Vegfr3 activity may be dispensable for facial lymphatic specification in the zebrafish [29]. Further work, however, is required to understand why this distinction exists between trunk and facial lymphatic specification.

The complex facial lymphatic network in zebrafish was first described in 2012 [32], and initial characterisation of this network showed that while the facial lymphatic sprout (FLS) arises from the common cardinal vein (CCV), it subsequently appears to acquire lymphatic progenitors from two other sources: firstly from another facial vein, called the primary head sinus (PHS), and secondly from a population of highly migratory *lyve1b*-positive cells termed the ventral aorta lymphangioblast (VA-L). The VA-L was first observed near the ventral aorta, and currently, there is no clear evidence that it is derived from a vein [32]. The facial lymphatics are therefore an ideal vascular network to investigate whether a complex lymphatic network can form from distinct venous and non-venous progenitor populations.

In this study, we identify with single-cell resolution a definitive, non-venous lymphatic progenitor in zebrafish. We confirm that the zebrafish facial lymphatic is formed from three distinct Prox1-positive lymphatic progenitor populations within the CCV, PHS and VA-L. Lymphangioblast contributions from these populations are tightly regulated at both a spatial and temporal level. The facial lymphatic forms through a relay-like mechanism, where vessel migration involves the sequential addition of lymphangioblasts to the growing vascular tip; first from the CCV, then the PHS and finally the VA-L. Finally, we also provide evidence that the VA-L does not have a venous origin; instead, it arises as an angioblast population that forms near the ventral aorta. This work supports the "dual origin" theory of lymphatic vessel development by providing evidence of a lymphatic progenitor that is not derived from an existing vessel.

Results

Early facial lymphatic development requires lymphangioblast contributions from anatomically distinct sources

Previous time-lapse studies suggested that the initial CCV-derived FLS appeared to recruit lymphangioblasts (defined here as migratory lymphatic progenitor cells) from two other sources: the PHS, between 42 and 48 hpf, and the VA-L, between 54 and 60 hpf [32] (Fig 1A and B). However, the manner in which these distinct lymphangioblast populations were coalescing to form the facial lymphatic network remained unclear. We generated a photoconvertible *lyve1b:Kaede* transgenic which recapitulated the expression of previously generated *lyve1b:EGFP*^{nz101} transgenic (Appendix FigS1A–C). While *lyve1b:Kaede* expression is initially weak at 36 hpf, photoconversion at this time allowed us to trace ~96% of *lyve1b*-positive cell populations to at least 24 h beyond the initial photoconversion of Kaede (Appendix Fig S2A–C and G). By photoconverting either the CCV or the PHS at 36 hpf, we confirmed that the CCV is the first to contribute lymphangioblasts to the initial facial lymphatic sprout (FLS) at 36 hpf (Fig 1C). By 48 hpf, lymphangioblast contributions from the CCV did not extend to the distal tip of the FLS, comprising only the proximal portion of the FLS, and this is still evident at 60 hpf (Fig 1D and E; Movie EV1). At this time, the remainder of the FLS is derived from the PHS (Fig 1F and G; Movie EV2). Photoconversion of the dorsal half of the VA-L at 54 hpf confirmed that this cell population provides further lymphangioblasts to the tip of the developing lateral facial lymphatic (LFL) by 72 hpf (Fig 2A and B). However, the ventral portion of the VA-L does not contribute to facial lymphatic development; instead, this migrates anteromedially and fuses to its contralateral counterpart along the ventral midline to form the anterior end and lateral branches of the hypobranchial artery (HA; Fig 2C and D). This suggests that despite its name, the VA-L is not entirely comprised of lymphangioblasts as it also contributes to blood vessel development. The HA carries blood from the first aortic arch, through the jaw and back to the sinus venosus [33,34]. Using both venous (*lyve1b:DsRed* or *flt4:mCitrine*) and arterial (*flt1:tdTomato*) enriched transgenes, we observed that the HA displays both arterial and venous identities (Fig EV1A–F). However, the medial portion of the HA, which joins to the sinus venosus, displays higher levels of venous transgene expression (Fig EV1B and D), whereas the arterial-enriched transgene is more strongly expressed in the bifurcating lateral branches, which join to the aortic arches and are contributed by the ventral VA-L (Fig EV1E). Overall, we confirmed via lineage tracing that three distinct sources, CCV-derived lymphangioblasts (CCV-Ls) at 36 hpf, PHS-derived lymphangioblasts (PHS-Ls) by 48 hpf and the VA-L by 72 hpf, contribute to the developing FLS.

At 72 hpf, once the FLS has fused to the VA-L, it is termed the lateral facial lymphatic (LFL). Subsequently, the otolithic lymphatic vessel (OLV) sprouts dorsally from the LFL and develops posterior to the otolith between 60 and 84 hpf, while the medial facial lymphatic (MFL) and lymphatic branchial arches (LAAs) sprout ventromedially from the LFL by 96 hpf (Fig 1B). To determine whether there were any additional lymphangioblast sources contributing to the development of the OLV and MFL, we photoconverted the LFL at either 60 or 72 hpf. This revealed that, up to 120 hpf, the OLV (Fig EV2A and B) and the MFL (Fig EV2C and D) are solely derived from the LFL. In

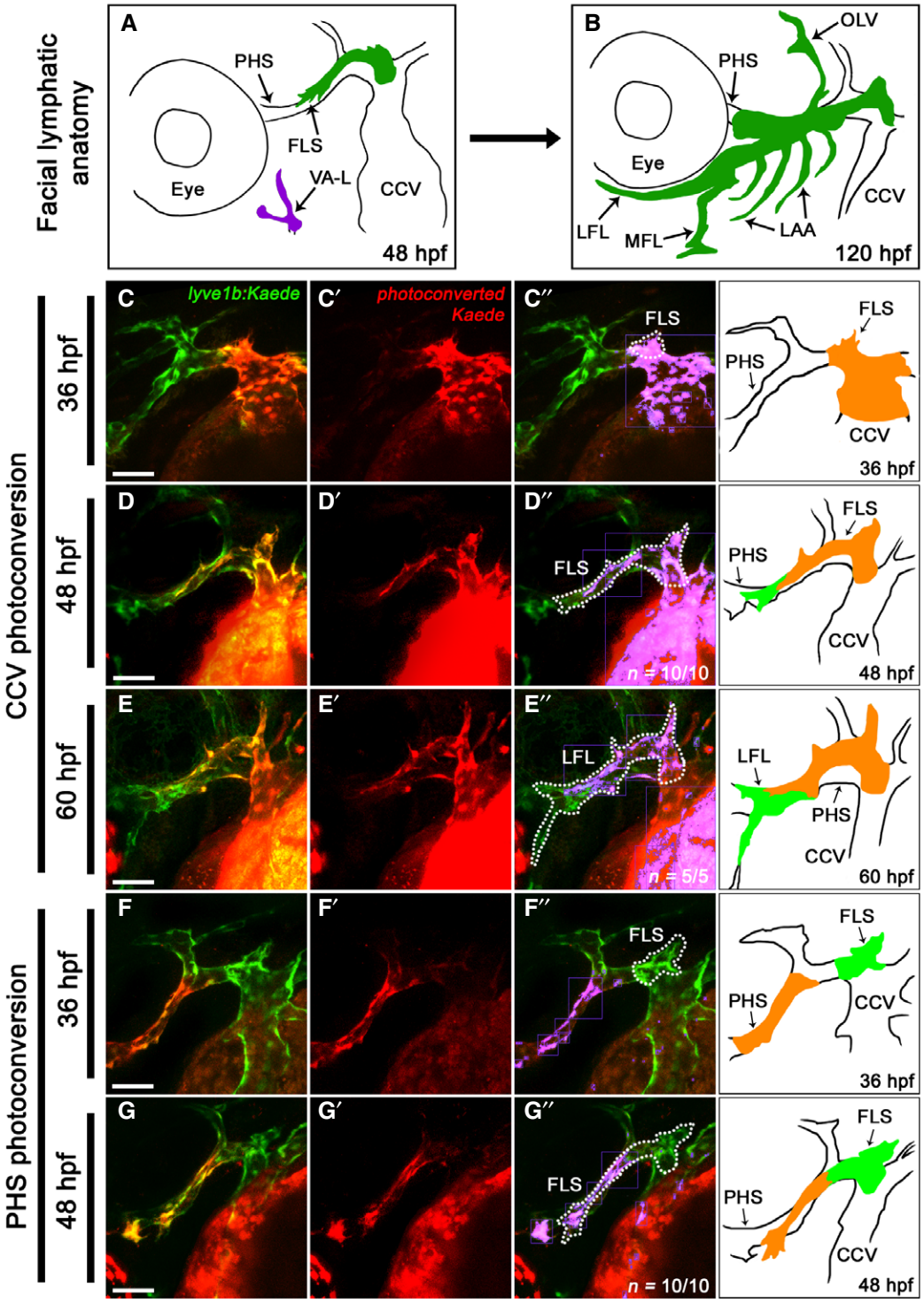

Figure 1. Early facial lymphatic development requires lymphangioblast contributions from anatomically distinct vessels.

A, B Schematic diagrams of the zebrafish facial lymphatic and cranial vessel anatomy at 48 hpf (A) and 120 hpf (B).

C–G" Lateral images of the cranial vessels in *lyve1b:Kaede* transgenic embryos with the CCV photoconverted at 36 hpf (C) and followed through to 48 hpf (D) and 60 hpf (E), while in a separate larva, the PHS has been photoconverted at 36 hpf (F) and followed to 48 hpf (G). Unconverted vessels are shown in green (C–G), while photoconverted vessels are shown in red (C'–G'). The extent of lymphangioblast contribution from each source is further clarified by false colouring the overlap between red and green fluorescence (purple), with the FLS demarcated (dotted line) from the adjacent primary veins (C"–G"). Schematic included for anatomical reference.

Data information: CCV, common cardinal vein; FLS, facial lymphatic sprout; hpf, hours post-fertilisation; LAA, lymphatic branchial arches; LFL, lateral facial lymphatic; MFL, medial facial lymphatic; OLV, otolithic lymphatic vessel; PHS, primary head sinus; VA-L, ventral aorta lymphangioblast. Scale bar = 50 μm.

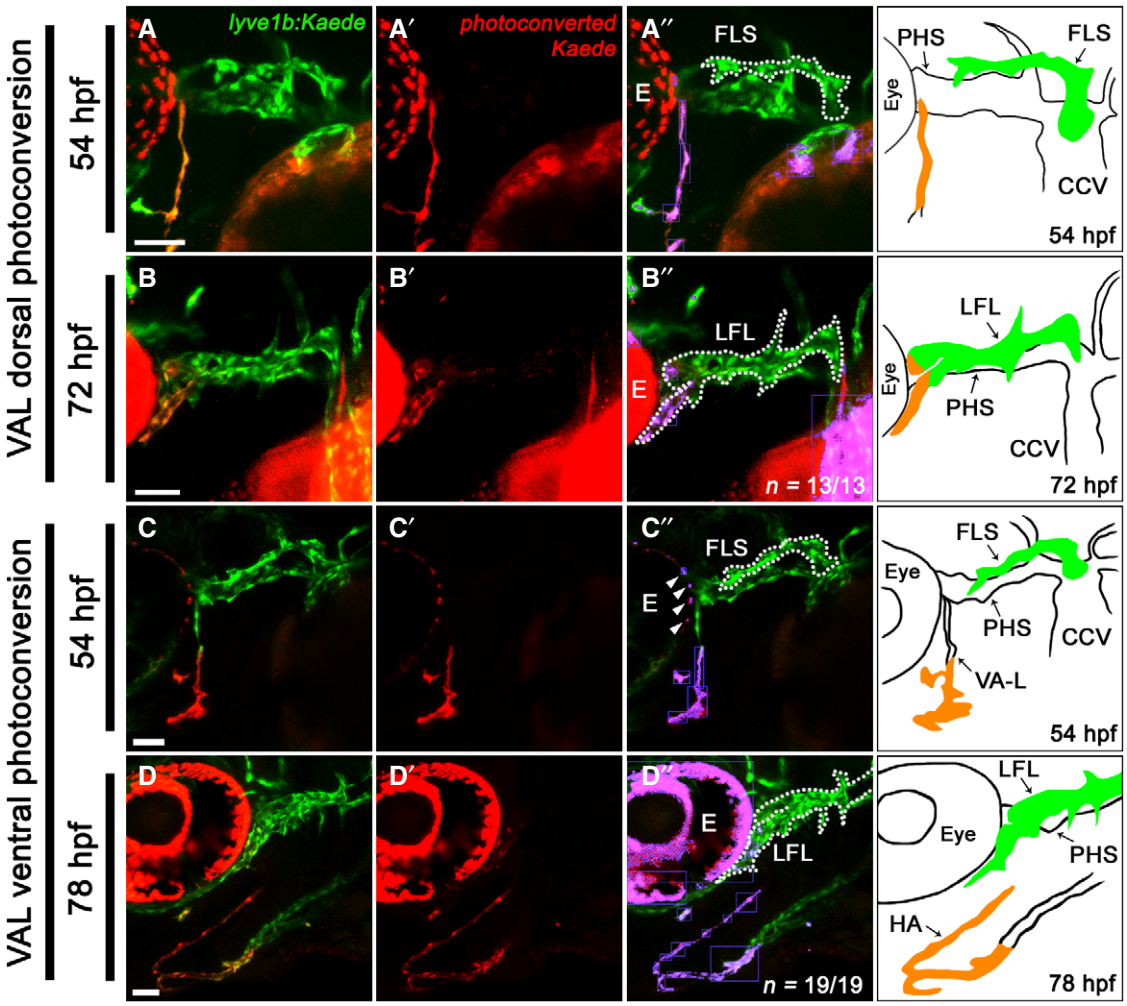

Figure 2. The VA-L contributes progenitors to both the facial lymphatic and the hypobranchial artery.

A–D″ Ventrolateral (A, C, D) and lateral (B) images of the cranial vessels in *lyve1b:Kaede* transgenic embryos with the dorsal (A) and ventral (C) portions of the VA-L photoconverted at 54 hpf and followed through to 72 hpf (B) and 78 hpf (D). Unconverted vessels are shown in green (A–D), while photoconverted vessels are shown in red (A′–D′). The extent of lymphatic and arterial contribution from the VA-L to the LFL (B″) or HA (D″) is further clarified by false colouring the overlap between red and green fluorescence (purple), with the FLS (A″, C″) and LFL (B″, D″) demarcated (dotted line) from the adjacent vessels. Schematic included for anatomical reference. Note, for all images, the overlap of red and green fluorescence in the eye (labelled E) is due to a combination of natural pigmentation and auto-fluorescence and is not indicative of photoconverted cells (C″, white arrowheads).

Data information: CCV, common cardinal vein; FLS, facial lymphatic sprout; HA, hypobranchial artery; hpf, hours post-fertilisation; LFL, lateral facial lymphatic; PHS, primary head sinus; VA-L, ventral aorta lymphangioblast. Scale bar = 50 μm.

addition, the LFL requires no further lymphangioblasts to complete its extension towards the jaw (Fig EV2E and F). Taken together, late facial lymphatic development appears to rely solely on existing lymphangioblasts within the LFL to form the OLV and MFL, and to complete the growth of the LFL.

Spatiotemporal distribution of facial lymphatic progenitors

Given that distinct lymphangioblast populations contribute to the developing facial lymphatic, we next wanted to investigate how lymphatic progenitor populations are distributed and patterned throughout the head prior to forming the FLS. Using Prox1 immunofluorescence staining in a *lyve1b:EGFP* transgenic background, we were able to identify Prox1$^+$/*lyve1b*$^+$ lymphatic progenitors. At the onset of facial lymphatic development (36 hpf), lymphatic progenitors are focused to a single point in the dorsolateral region of the CCV (Fig 3A). These then transition into migrating lymphangioblasts by 42 hpf, forming the initial FLS. In addition, Prox1 expression in CCV lymphangioblasts (CCV-Ls) appears to be polarised, with cells closer to the growing tip displaying a higher level of Prox1 expression than those closer to the CCV (Fig 3B). By contrast, lymphatic progenitors found in the PHS at 36 hpf are initially positioned along the entire length of the vein in an interspersed manner (Fig 3C). Six hours later, these cells form two distinct lymphatic progenitor domains: one at the anterior end of the PHS, the anterior PHS-derived lymphatic progenitor domain (PHS-LP$_A$), and one posterior to this, the posterior PHS-derived lymphatic progenitor domain (PHS-LP$_P$; Fig 3D). By 48 hpf, PHS-LP$_P$, the

domain closest to the CCV, has sprouted from the PHS and become part of the FLS (Fig 3E). Unlike the CCV-L and PHS-Ls, the VA-L is Prox1-negative at 36 hpf (Fig 3F), not acquiring lymphangioblast identity until 42 hpf when Prox1 expression becomes evident (Fig 3G). Later at 48 hpf, only the dorsal portion of the VA-L that contributes to the facial lymphatics contains Prox1-positive lymphangioblasts, while the ventral portion that contributes to HA formation remains Prox1-negative (Fig 3H). Altogether, the distinct spatiotemporal pattern of lymphatic progenitors in the CCV, PHS and VA-L confirms their roles in contributing lymphangioblasts to the growing facial lymphatic.

Vegfr3 signalling is required for lymphatic progenitor domain formation in the PHS but not the CCV or the VA-L

We wanted to compare the role of Vegfr3 signalling on lymphatic specification in the CCV with that of the PHS, including its effect on the formation of the PHS-LP_A and PHS-LP_P domains. In order to disrupt the Vegfr3 signalling axis, we analysed either *ccbe1* morphants or embryos injected with a dominant negative inhibitor of Vegfr3 signalling (*sFLT4* mRNA) [35], approaches previously shown to inhibit FLS formation [28]. We confirmed the efficacy of our knockdowns by quantitating the length of the FLS at 48 hpf and observed robust inhibition of sprouting following injection of either *ccbe1* MO or *sFLT4* mRNA (Appendix Fig S3A–F). We found that while both *ccbe1* morphants and *sFLT4* mRNA-injected embryos displayed a marked reduction in the number of PHS Prox1-positive lymphatic progenitors at 36 hpf (Fig 4B, F, I and J) and 42 hpf (Fig 4D, H, I and J) compared to controls (Fig 4A, C, E, G, I and J), they nevertheless still had Prox1-positive cells present in the PHS, indicating that some lymphatic specification had occurred. Importantly, the total numbers of PHS endothelial cells (ECs) in either *ccbe1* morpholino or *sFLT4*-injected fish were unchanged when compared to control morpholino-injected and uninjected larvae (Fig 4K), indicating that blood vascular development proceeded normally. Of note, at 42 hpf, *ccbe1* morphants and *sFLT4*-injected embryos failed to form the distinctive PHS-LP domains (Fig 4D and H). By contrast, although *ccbe1* MO or *sFLT4* injections inhibited facial lymphatic sprouting at 36 hpf—evident by the reduced number of cells in the dorsolateral CCV region (Fig 4Q) and inhibition of FLS development (Appendix Fig S3)—it did not reduce the percentage of dorsolateral CCV ECs that are Prox1-positive lymphatic progenitors compared to controls (Fig 4L–P), which is consistent with what is seen in *flt4* mutants [29]. In addition, the VA-L in *ccbe1* morphants and *sFLT4*-injected embryos also remained Prox1-positive at 54 hpf (Fig 4R–U), indicating that, like lymphatic progenitors in the CCV, Vegfr3 signalling is not required for the initial induction and maintenance of Prox1 expression in the VA-L. Taken together, these results suggest that Vegfr3 signalling is required for the formation of lymphatic progenitor domains within the PHS, but not for the initial specification of facial lymphatic progenitors.

The early facial lymphatic forms through the sequential addition of lymphangioblasts to the growing tip

Given that lymphangioblast populations from the CCV, PHS and the VA-L come together to form the FLS, we wished to examine the process in real time to better understand the migratory behaviour of

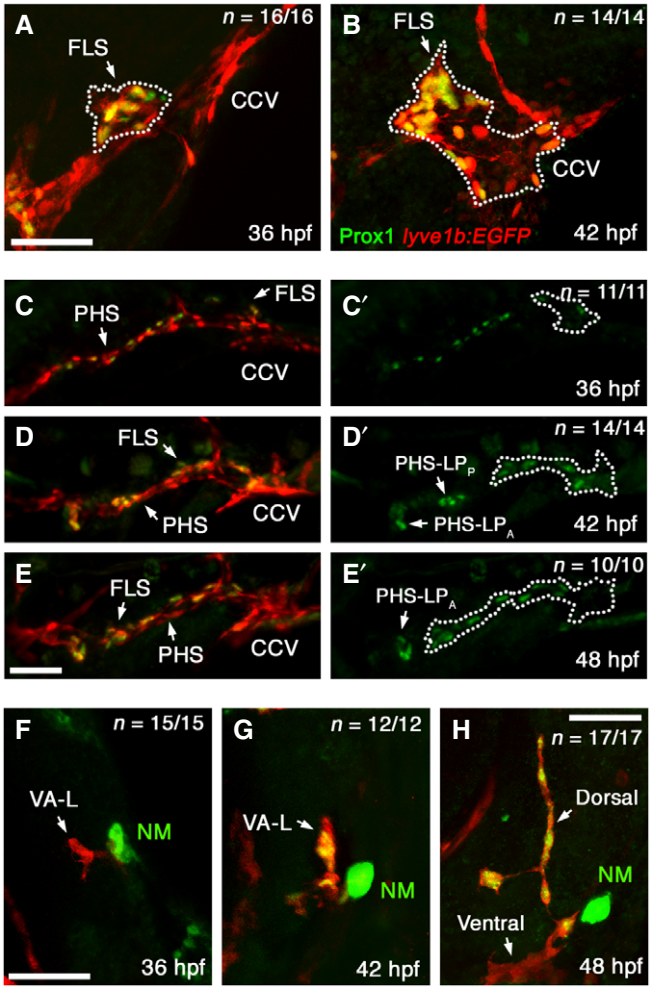

Figure 3. Spatiotemporal distribution of lymphatic progenitors in the cranial vessels.

A–H Lateral images of the CCV fixed at 36 hpf (A) and 42 hpf (B), of the PHS at 36 hpf (C), 42 hpf (D) and 48 hpf (E) and of the VA-L at 36 hpf (F), 42 hpf (G) and 48 hpf (H) in *lyve1b:EGFP* fish that have been fluorescently immunostained with anti-PROX1 (green) and anti-GFP (red). PHS Prox1 staining shown alone for all timepoints (C′–E′) with the FLS demarcated (dotted line) from the adjacent vessels, and the positions of the PHS-LP_P and PHS-LP_A indicated. Note the Prox1-positive (green), GFP-negative structure near to the VA-L is a *prox1*-expressing neuromast (NM).

Data information: CCV, common cardinal vein; FLS, facial lymphatic sprout; hpf, hours post-fertilisation; NM, neuromast; PHS, primary head sinus; PHS-LP_A, anterior primary head sinus lymphatic progenitor domain; PHS-LP_P, posterior primary head sinus lymphatic progenitor domain; VA-L, ventral aorta lymphangioblast. Scale bar = 50 μm.

specific lymphangioblast populations. Using time-lapse imaging of *lyve1b:EGFP;kdrl:nlsmCherry* compound transgenics, we were able to track the events leading to, and after, fusion of the FLS tip—initially comprised of CCV-Ls—to the PHS-Ls sprouting out of the PHS-LP_P (Movie EV3), and from the FLS tip—now comprised of PHS-Ls—to the VA-L (Movie EV4). We also quantitated the migratory behaviour of the lymphangioblasts involved by tracking the leading cell of the CCV-L-derived FLS tip, the PHS-L-derived FLS tip and the VA-L 3–4 h before and 3–4 h following fusion to the subsequent lymphangioblast

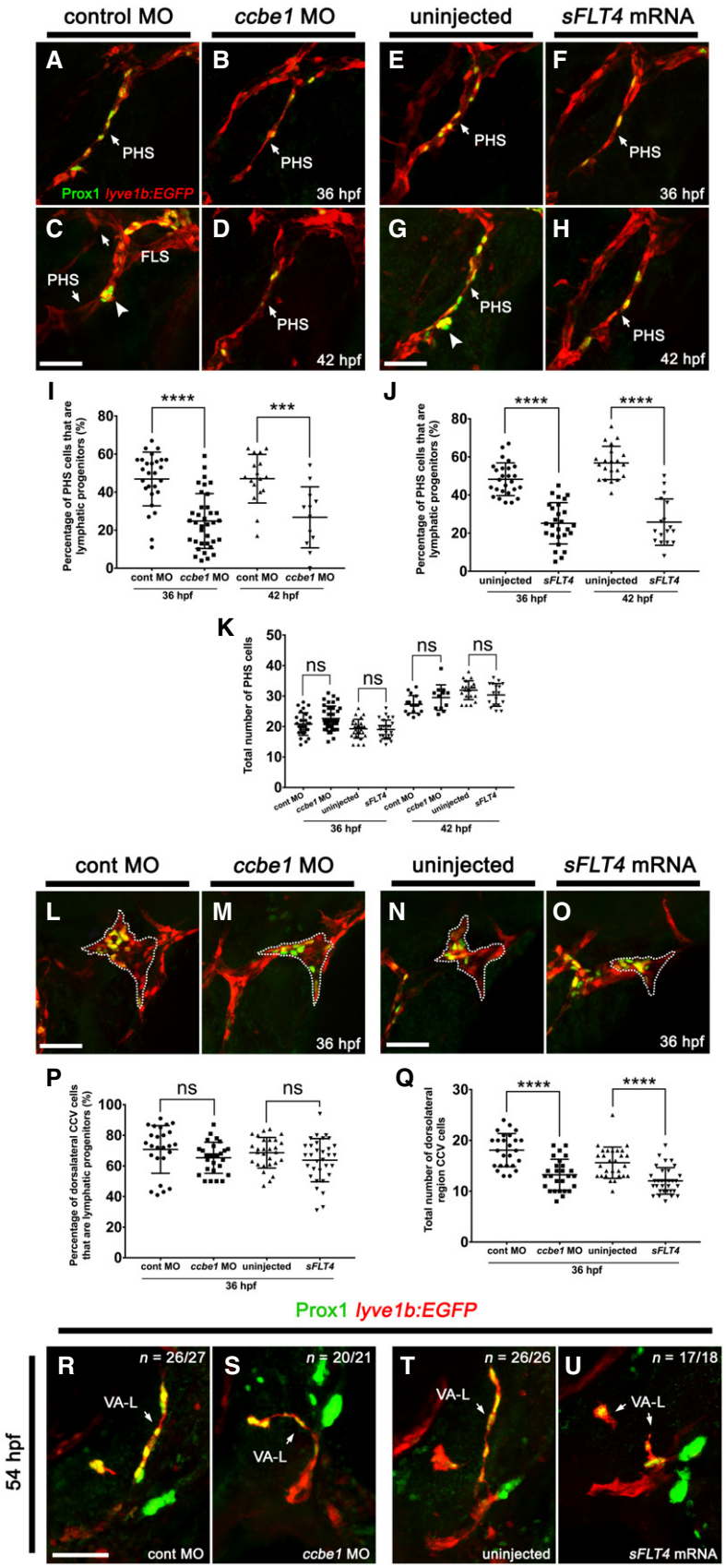

Figure 4.

Figure 4. Vegfr3 signalling is not required for facial lymphatic progenitor formation.

A–H Lateral images of the PHS fixed at 36 hpf (A, B, E, F) and 42 hpf (C, D, G, H) in *lyve1b:EGFP* fish that have been fluorescently immunostained with anti-PROX1 (green) and anti-GFP (red). These show a decrease in the number of Prox1-positive PHS ECs in the *ccbe1* morpholino-injected (B, D) and *sFLT4* mRNA-injected embryos (F, H) compared with control morpholino-injected (A, C) and uninjected embryos (E, G). At 42 hpf, *ccbe1* morpholino-injected embryos (D) and *sFLT4* mRNA-injected embryos (H) lack the PHS-LP domains present in the control embryos (C, G; large arrow heads).

I, J Quantitation of the percentage of PHS ECs that are lymphatic progenitors relative to the total number of PHS ECs in control morpholino-injected embryos at 36 hpf (n = 27) and 42 hpf (n = 17) and *ccbe1* morpholino-injected embryos at 36 hpf (n = 36) and 42 hpf (n = 12) (I) or in uninjected embryos at 36 hpf (n = 27) and 42 hpf (n = 21) and *sFLT4* mRNA-injected embryos at 36 hpf (n = 26) and 42 hpf (n = 17) (J).

K Quantitation of the total number of PHS ECs in control morpholino-injected embryos at 36 hpf (n = 27) and 42 hpf (n = 17) and *ccbe1* morpholino-injected embryos at 36 hpf (n = 36) and 42 hpf (n = 12) or in uninjected embryos at 36 hpf (n = 27) and 42 hpf (n = 21) and *sFLT4* mRNA-injected embryos at 36 hpf (n = 26) and 42 hpf (n = 17).

L–O Lateral images of the FLS (L, N; dotted line) or dorsolateral CCV region from where the FLS normally sprouts (M, O; dotted line) fixed at 36 hpf in *lyve1b:EGFP* embryos that have been fluorescently immunostained with anti-PROX1 (green) and anti-GFP (red). These show no change in the number of Prox1-positive lymphatic progenitors in the *ccbe1* morpholino-injected (M) and *sFLT4* mRNA-injected (O) embryos compared with control morpholino-injected (L) and uninjected (N) embryos.

P Quantitation of the percentage of dorsolateral CCV ECs that are lymphatic progenitors relative to the total number of dorsolateral CCV ECs in control morpholino-injected (n = 26), *ccbe1* morpholino-injected (n = 27), uninjected (n = 28) and *sFLT4* mRNA-injected embryos (n = 32).

Q Quantitation of the total number of dorsolateral region CCV ECs in 36 hpf embryos that were uninjected or injected with control morpholino (n = 26), *ccbe1* morpholino (n = 27) or *sFLT4* mRNA (n = 32).

R–U Dorsolateral images of the VA-L fixed at 54 hpf in *lyve1b:EGFP* larva that have been fluorescently immunostained with anti-PROX1 (green) and anti-GFP (red). These show that lymphatic progenitor formation still occurs within the VA-L in *ccbe1* morpholino-injected (S) and *sFLT4* mRNA-injected embryos (U), with Prox1 expression resembling that of controls (R, T).

Data information: Error bars represent standard deviation; ****$P < 0.0001$, ***$P < 0.001$, ns = non-significant by one-way ANOVA. CCV, common cardinal vein; EC, endothelial cell; FLS, facial lymphatic sprout; hpf, hours post-fertilisation; PHS, primary head sinus; PHS-LP, primary head sinus-derived lymphatic progenitor; VA-L, ventral aorta lymphangioblast. Scale bar = 50 μm.

populations. Early in FLS development, we found that the CCV-Ls idle for some time and only migrate rapidly towards the PHS-LP_P and PHS-LP_A domains at around 42 hpf (Fig 5A; Movie EV3). As the CCV-L-derived FLS approaches, cells within the PHS-LP_P increase in number by undergoing 1–2 rounds of cell division before sprouting to fuse with the arriving facial lymphatic tip at 48 hpf (Fig 5B). At this juncture, the initial CCV-Ls that were leading the FLS essentially cease migration (Fig 5C and D), and the PHS-Ls (derived initially from the PHS-LP_P) form the distal portion of the FLS and migrate towards the VA-L (Fig 5E and F; Movie EV4). Meanwhile, a secondary sprout from the distal end of the FLS—comprised of PHS-LP_P cells—fuses to the PHS-LP_A domain by 52 hpf (Fig 5E; Movie EV4). Similar to the initial CCV-Ls, the VA-L remains idle during the 12-h period from the onset of facial lymphatic development to the FLS fusing to the PHS-Ls. Subsequent to this fusion event, the VA-L begins migrating towards the PHS-L-derived FLS tip, with the two populations fusing together by 55 hpf (Fig 5E; Movie EV4). Upon fusion, the PHS-L-derived FLS tip and the VA-L stall migration (Fig 5C, G and H) as several rounds of cell division occur (Fig 5F; Movie EV4), before the now LFL resumes migration along the ventral wall of the eye and towards the jaw. Further evidence supporting the timing of fusion events comes from total facial lymphatic cell count over time, which shows that although cell division plays a role in contributing to the increase in facial LECs, the greatest increase in cell number comes from the PHS-Ls and VA-L fusing to the FLS (Appendix Fig S4). Altogether, facial lymphatic development involves the sequential addition of lymphangioblasts, first from the CCV, then the PHS and finally the VA-L, to the growing tip, creating a "relay-like" mechanism which drives the formation of the facial lymphatics.

The VA-L does not arise from a vein

While the VA-L provides lymphangioblasts to the developing facial lymphatic, the origin of this cell population remains unknown. As the VA-L is *lyve1b*-positive from 36 hpf onwards [32], we initially surmised that its origin could be a previously uncharacterised vein located within the vicinity of the VA. To explore this possibility, we developed a *kdrl:nlsKaede* transgenic to lineage trace any *kdrl*-expressing structure near the VA that could give rise to the VA-L. Our *kdrl:nlsKaede* transgenic recapitulated the expression of the previously published *kdrl:nlsmCherry*^{nz49} transgenic (Appendix Fig S1D–F), and photoconversion at 24 hpf allowed us to detect at least 90% of photoconverted cells 24–48 h beyond the initial photoconversion of Kaede (Appendix Fig S2D–G). We photoconverted various *kdrl*-expressing tissues at 24 hpf and traced the photoconverted Kaede to 54 hpf, a timepoint when the VA-L is clearly visible. However, with this photoconversion regimen, we were unable to trace the VA-L progenitor from either the CCV, PHS, optic veins, endocardium, lateral dorsal aorta or pharyngeal endoderm (Fig EV3A–F and H–M). Furthermore, even when photoconverting the entire *kdrl*-expressing population within the head at 24 hpf, we did not see any photoconverted cells within the VA-L (Fig EV3G and N), suggesting that the VA-L acquires *kdrl:nlsKaede* expression after this timepoint. However, we noted that at 34 hpf, there was a small cluster of 4–5 *kdrl*-positive cells closely associated with the ventral region of the VA, and by photoconverting these cells at 34 hpf, we were able to identify this as the earliest visible *kdrl*-positive form of the VA-L (Fig 6A and B). We then performed time-lapse imaging in this area between 31 and 35.8 hpf in *kdrl:EGFP;kdrl:nlsmCherry* compound transgenics and found that the VA-L begins expressing *kdrl:nlsmCherry* between 32 and 33 hpf in a manner that was independent of any neighbouring *kdrl*-expressing tissues (Fig 6C; Movie EV5); despite closely associating with the VA, the VA-L was never seen to form a connection with the VA (Fig 6D; Movie EV6), supporting previous data that showed that the VA-L does not express an arterially enriched transgene (*flt1:YFP*^{hu4624}) [23,32]. We also investigated the possibility that myeloid cells could give rise to the VA-L, or that they may play an indirect role in mediating its formation. We performed double morpholino knockdown of *pu.1* and *csfr3*, a combination known to broadly inhibit

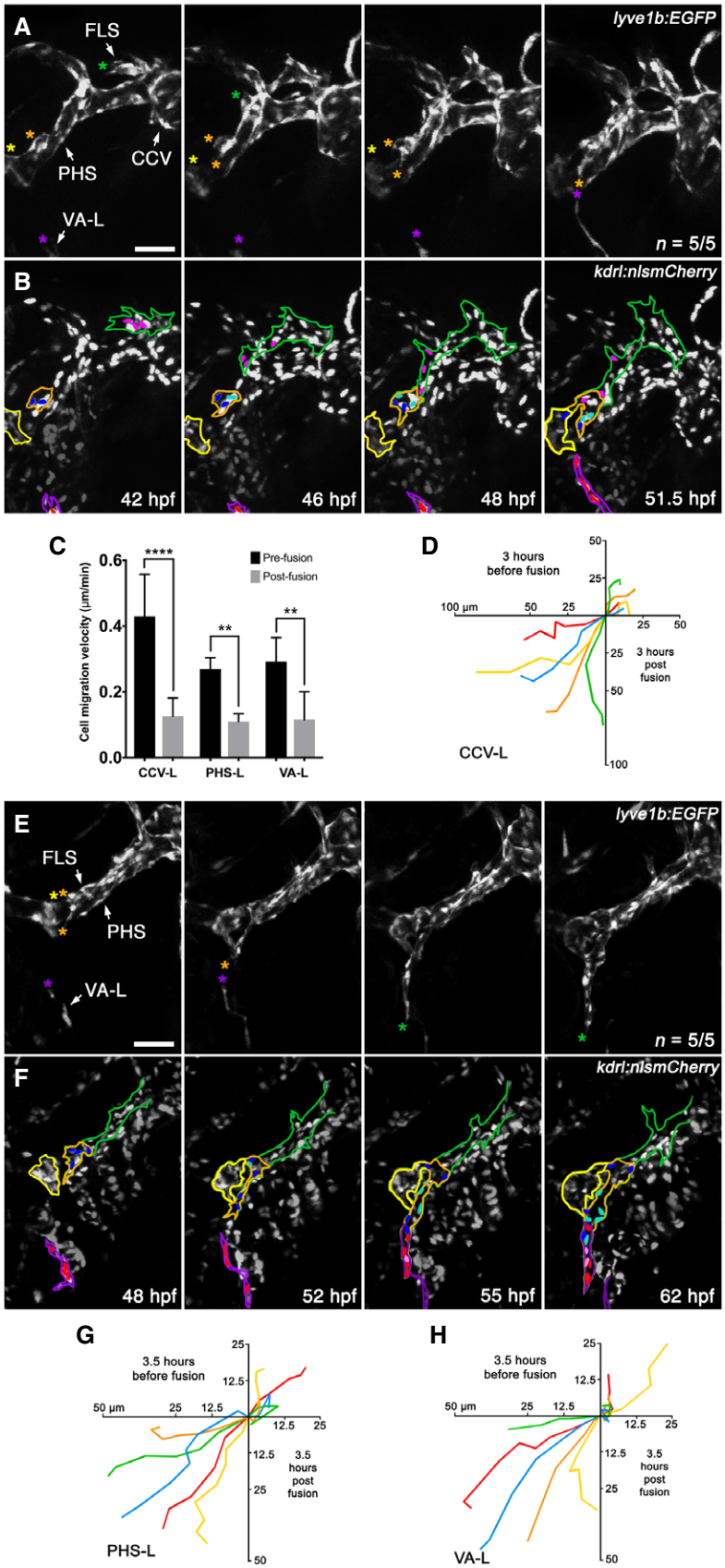

Figure 5.

Figure 5. The early facial lymphatic forms through the sequential addition of lymphangioblasts to the growing tip.

A, B Still images from Movie EV3 of early facial lymphatic development in a *lyve1b:EGFP* (A), *kdrl:nlsmCherry* (B) compound transgenic from 42 to 51.5 hpf, with the CCV-L-derived leading tip cell (green asterisk), the PHS-LP domains (orange and yellow asterisk) and the distal tip of the VA-L (purple asterisk) highlighted (A). Between 42 and 46 hpf, the PHS-LP_P (orange outline) cells divide (dark blue parent cells, light blue daughter cells) before sprouting as lymphangioblasts from the PHS and fusing with the tip (pink cells) of the CCV-derived FLS (green outline) at 48 hpf (B). Cells (red) within the VA-L (purple outline) can also be seen migrating towards the now PHS-L-derived FLS tip by 48 hpf. The PHS-LP_A is also shown (yellow outline).

C Quantitation of leading lymphangioblast velocity (μm/min) before and after fusion with another lymphangioblast [CCV-L-derived FLS tip (pink cells) to PHS-L (B, blue cells; n = 5/5) and PHS-L-derived FLS tip (blue cells) to VA-L (F, red cells; n = 5/5)] or by the VA-L to the PHS-L-derived FLS tip (B, n = 5/5).

D Cell migration tracks where each coloured track depicts the distance (μm) travelled over 3 h by the leading tip cell in a separate animal before and after fusion with the CCV-L-derived FLS tip (pink cells) and the PHS-Ls (B, blue cells; n = 5/5).

E, F Still images from Movie EV4 of facial lymphatic development in a *lyve1b:EGFP* (C), *kdrl:nlsmCherry* (D) compound transgenic from 48 to 62 hpf showing that after the CCV-derived FLS fuses to the PHS-L, these take over as the leading tip cells (orange asterisks), with one PHS-L migrating anteriorly to fuse with PHS-LP_A (yellow asterisk), and others migrating ventrally to fuse with the VA-L (purple asterisk) (C). After the PHS-derived portion (orange outline) of the FLS (green outline) fuses to the VA-L (purple outline), migration of the entire facial lymphatic pauses to allow for lymphangioblast proliferation (dark blue and red parent cells, light blue and pink daughter cells) before resuming migration anteriorly along the ventral base of the eye (D).

G, H Cell migration tracks where each coloured track depicts the distance (μm) travelled over 3.5 h by the leading tip cell in a separate animal before and after fusion with another lymphangioblast [PHS-L-derived FLS tip (blue cells) to VA-L (F, red cells; n = 5/5)] or by the VA-L to the PHS-L-derived FLS tip (F, n = 5/5).

Data information: Error bars represent standard deviation; ****$P < 0.0001$, **$P < 0.01$ by unpaired Student's t-test. CCV, common cardinal vein; CCV-L, common cardinal vein-derived lymphangioblast; FLS, facial lymphatic sprout; hpf, hours post-fertilisation; PHS, primary head sinus; PHS-L, primary head sinus-derived lymphangioblast; PHS-LP_A, anterior primary head sinus lymphatic progenitor domain; PHS-LP_P, posterior primary head sinus lymphatic progenitor domain; VA-L, ventral aorta lymphangioblast. Scale bar = 50 μm.

myelopoiesis [36], and saw that the VA-L forms normally after myeloid cells were depleted (Appendix Fig S5A–D). Overall, our data suggest that the VA-L does not originate from any existing *kdrl*-positive vessels or myeloid cells in this region; instead, it begins to independently express *kdrl* as an isolated cell population.

The VA-L originates from a single late-forming angioblast

As the VA-L appears to turn on *kdrl* expression later than the established vessels in the head, we sought to use a vascular progenitor marker that precedes the expression of *kdrl*, such as *etv2*, to identify what, if any, angioblast population it may be affiliated with. Time-lapse imaging the angioblast-marking *etv2:EGFP* transgenic [37] crossed with *kdrl:nlsmCherry,* revealed that the VA-L begins expressing *etv2:EGFP* as a single isolated cell as early as 29 hpf in the avascular perivitelline space above the anterodorsal yolk sac region (Fig 6E; Movie EV7). This migrates ventrally towards the VA, and once adjacent to the VA, begins to express *kdrl:nlsmCherry* at 33 hpf while undergoing rounds of cell division (Fig 6E'; Movie EV7). To further confirm that the VA-L arises from this *etv2*-expressing angioblast, we photoconverted it at 29 hpf using an *etv2:Kaede* transgenic (Fig 6F) [38], which—despite mosaic expression of this transgene (Appendix Fig S2H–J)—was subsequently traced to the VA-L at 54 hpf (Fig 6G). We used cell ablation to further confirm our hypothesis that the VA-L arises from this angioblast cell and that it then fuses with the FLS to contribute to facial lymphatic formation by 60 hpf. We used a 405 nm SIM scanning laser to ablate the angioblast cell on the left lateral side of the embryo at 30 hpf (Fig 7A and B). We found that the VA-L was not present at 54 hpf on the ablated side, but was still seen on the contralateral unablated side (Fig 7C and D), which was used as an internal control. By 78 hpf, both the LFL and the HA were significantly affected by VA-L ablation; the LFL was not extending towards the eye (Fig 7E and F), and the left lateral branch of the HA, which connects to the first aortic arch, was missing on the ablated side compared to the unablated contralateral side (Fig 7G). In addition, both the length of the LFL and the number of cells within the LFL were significantly decreased on the ablated side compared to the contralateral side (Fig 7H and I). Overall these ablation studies confirm that this isolated *etv2*-expressing angioblast population gives rise to the VA-L, which subsequently contributes to both LFL and HA formation.

To further characterise the genes involved in forming this VA-L-contributing angioblast population, we also looked at a second angioblast marker, *fli1*. Via time-lapse imaging, we observed *fli1a:nEGFP* turning on in the isolated VA-L cell population at approximately 30–31 hpf, followed shortly after by *kdrl:mCherry* (Movie EV8). The VA-L angioblast population therefore displays delayed induction of *etv2*, *fli1* and *kdrl*, with expression of these transgenes in this population occurring 15–20 h after they are first observed in the developing embryo [37,39]. Given that this angioblast population is forming well after other angioblasts involved in cranial vasculogenesis, we wondered whether formation of the VA-L is still regulated by *clo/npas4l*, the master regulator of endothelial and haematopoietic cell fate [40,41]. We injected a combination of ATG and splice-blocking *clo/npas4l* morpholinos [41] into *etv2:EGFP; kdrl:nlsmCherry* embryos and found that VA-L formation was sensitive to *npas4l* knockdown; although morphants formed some semblance of the cranial vessels, the VA-L progenitor was not present at 34 hpf (Fig EV4A and B), and the VA-L completely failed to form by 54 hpf (Fig EV4C and D). Furthermore, the morphant phenotype was found to be recapitulated in the mutant, with the VA-L absent in *clo/npas4l*^{s5} mutants at 34 (Fig EV4E and F) and 54 hpf (Fig EV4G and H). Overall, the VA-L does not sprout from an existing vein; instead, it arises from a single isolated *etv2/fli1/kdrl*-expressing angioblast that is dependent on *clo/npas4l* activity and its formation occurs well after the major cranial vessels have already been established.

Vegfr3 signalling is not necessary for VA-L formation but is required for VA-L migration

Given that lymphatic progenitor formation in the CCV and the PHS displayed differing sensitivity to knockdown of Vegfr3 signalling, we decided to test the role of this pathway in the formation of the VA-L. In order to abrogate Vegfr3 signalling, we

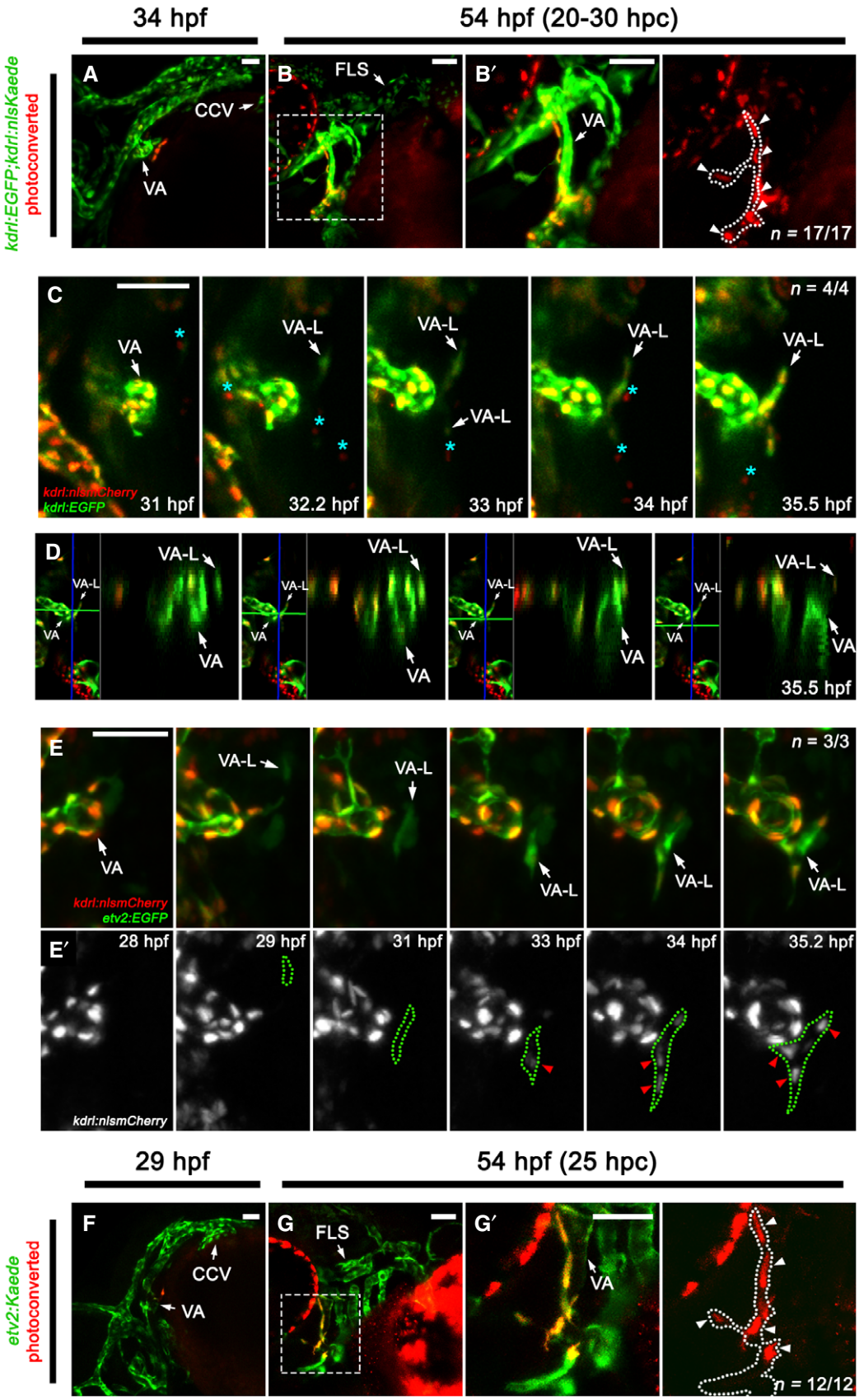

Figure 6.

Figure 6. The VA-L is not derived from a vein; instead, it arises independently from a single angioblast cell.

A–B' Lateral (A) and ventrolateral (B, B') images of the cranial vessels in *kdrl:nlsKaede;kdrl:EGFP* embryos, with unconverted tissue shown in green (A, B) while photoconverted tissue is shown in red (B'). The early *kdrl*-positive VA-L was photoconverted in 34 hpf embryos (A) and followed through to 54 hpf (B, B'). (B') is a higher magnification image of the box in (B) and is accompanied by a red channel only (traced photoconverted cells) image with the VA-L (dotted line) demarcated from the adjacent VA. The VA-L photoconverted cells are indicated by arrowheads.

C Still images from Movie EV5 of VA-L development in a *kdrl:EGFP;kdrl:nlsmCherry* compound transgenic from 31 to 35.5 hpf. This movie shows that the VA-L begins expressing *kdrl* just after 32 hpf, in a manner that is isolated and independent of any neighbouring *kdrl*-positive tissue or vessel. Putative *kdrl*-positive primitive myeloid cells (light blue asterisks) can also be seen migrating along the surface of the yolk in the immediate vicinity of the VA and VA-L.

D Still images from Movie EV6 depicting a 3D reconstruction of the 35.5 hpf timepoint from Movie EV5. A dorsal view that scrolls through the Y-stack of the VA-L is shown, which illustrates that the VA-L is closely associated with, but not connected to the VA.

E, E' Still images from Movie EV7 of VA-L development in an *etv2:EGFP* (E), *kdrl:nlsmCherry* (E') compound transgenic from 28 to 35.2 hpf. This movie shows that the VA-L begins expressing *etv2* (E) at 29 hpf and is independent of any neighbouring vessel. *kdrl* expression (red arrowheads) occurs 4 h later in the VA-L (demarcated by the green dotted line) (E').

F–G' Lateral images of the cranial vessels in *etv2:Kaede* embryos, with unconverted tissue shown in green (F, G) while photoconverted tissue is shown in red (G'). The earliest visible form of the VA-L was photoconverted at 29 hpf (F), then followed through to 54 hpf (G). (G') is a higher magnification image of the box in (G) and is accompanied by a red channel only (traced photoconverted cells) image with the VA-L (dotted line) demarcated from the adjacent VA, and VA-L photoconverted cells indicated (arrowheads).

Data information: CCV, common cardinal vein; FLS, facial lymphatic sprout; hpf, hours post-fertilisation; hpc, house post-conversion; VA, ventral aorta; VA-L, ventral aorta lymphangioblast. Scale bar = 50 μm.

separately injected either *ccbe1* morpholino or *sFLT4* mRNA into *etv2:EGFP* or *lyve1b:EGFP* fish. We found that in *ccbe1* morphants and *sFLT4*-injected fish, the VA-L was present but significantly shorter in length than that of controls from 48 hpf onwards (Fig EV4I–R), indicating that the VA-L fails to migrate dorsally in the absence of Vegfr3 signalling which is consistent with previous findings [32]. However, in both *ccbe1* morphants and *sFLT4*-injected fish, the initial formation and development of the VA-L until 48 hpf progresses normally, with the timing of the VA-L migration defect being concomitant with the expression of Prox1 in the dorsal region of the VA-L (Fig 3F–H). Overall, while Vegfr3 signalling is required for dorsal migration and expansion of the VA-L towards the developing FLS, it is not necessary for the formation of the VA-L or the initial induction and maintenance of Prox1 expression within the dorsal VA-L.

Discussion

Recent work in both mouse and zebrafish has given rise to the hypothesis that the origin and formation of the lymphatic vasculature is heterogenous between distinct vascular beds [42,43]. In this study, we show that the zebrafish facial lymphatic network is formed via mechanisms that are distinct from that of the zebrafish trunk lymphatic network. Using lineage tracing and live imaging techniques, we confirm that the initial facial lymphatic is formed by the relay-like coalescence of separate lymphangioblast populations arising from the CCV, PHS and VA-L (Fig 8). Finally, we demonstrate that the VA-L originates from a unique *clo/npas4l*-dependant angioblast population that arises late in development and does not sprout from an existing blood vessel, providing the first definitive evidence of a non-venous lymphatic progenitor in zebrafish. Throughout this study, we have named this non-venous lymphangioblast population the "ventral aorta lymphangioblast" (VA-L); however, it does not meet the definition of a lymphangioblast until it acquires Prox1 expression in the dorsal population at 42 hpf. Therefore, we propose to rename the initial *etv2/fli1/kdrl*-positive cell(s) that arise at 29 hpf in the anterodorsal perivitelline space the "ventral aorta angioblast" (VA-A), as this cell population is migratory, Prox1-negative and is able to give rise to both blood vascular and lymphatic progenitors. We also propose to limit the term "VA-L" to the dorsal, Prox1-positive portion of the VA-A that later contributes to the facial lymphatic (Fig 8).

The facial lymphatic has a non-venous progenitor

In the early 20th century, Sabin proposed the "venous" model of lymphatic origin [8], which is supported by contemporary lineage-tracing evidence showing that lymphatic progenitors are specified within and sprout from the veins of mice and zebrafish [11,12]. More recently, the "dual origin" theory, wherein a combination of venous and non-venous lymphatic progenitors form the lymphatic vasculature [13,14,16], has been gaining popularity following a series of Cre-LoxP lineage-tracing experiments in mice [17–19]. However, many of these studies have been contradictory [17,19,20,22], in part due to technical limitations in the genetic lineage-tracing techniques, and direct evidence of a non-venous lymphatic progenitor has remained elusive.

In this study, we have used a complementary approach involving high-resolution live cell imaging and cell ablation to show definitive evidence of a non-venous lymphatic progenitor. We show that the VA-L, which contributes lymphangioblasts to the facial lymphatic, does not sprout from any blood vessels in the head. Instead, it is derived from a unique *clo/npas4l*-dependant angioblast population we called the VA-A, which arises at 29 hpf and later contributes to both lymphatic and blood vascular development by 72 hpf. Previously, a specialised angioblast niche has been described in the ventral wall of the PCV that contributes progenitors to the zebrafish trunk lymphatics, subintestinal veins and supraintestinal arteries [24]. While this study demonstrated that lymphatic progenitors can differentiate directly from "angioblast cells" within a vein, these lymphatic progenitors are nevertheless still derived from PCV cells, making them by definition venous in origin. In support of this, previous live imaging studies have confirmed that the trunk lymphatics are derived solely from cells within the PCV [11,44].

The anterior lateral plate mesoderm (ALPM) gives rise to the angioblasts that form the cranial and facial vessels, heart

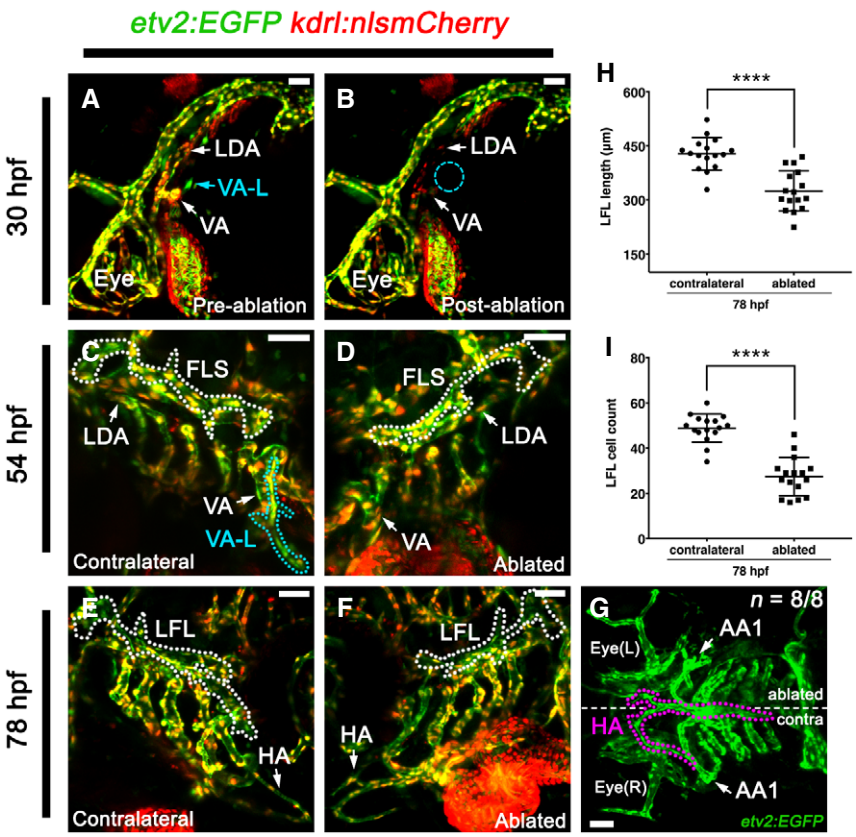

Figure 7. Ablating the *etv2*-expressing angioblast population on the anterodorsal yolk sac surface leads to loss of VA-L formation and defects in LFL and HA development.

A–G Lateral (A, B), ventrolateral (C–F) and ventral (G) images of the cranial vessels in an *etv2:EGFP;kdrl:nlsmCherry* compound transgenic embryo, which has had the *etv2*-expressing angioblast population (early VA-L) on the left lateral side of the yolk sac ablated. Images were taken at 30 hpf before (A) and after (B) ablation of the early VA-L, with the site of ablation indicated (B; blue dotted circle). Note that the LDA and VA adjacent to the VA-L become photobleached during the ablation process (B), however, these were not ablated as they can be seen developing normally at 54 hpf (D). Follow-up images were taken of both the contralateral (C, E) and ablated (D, F) sides of the embryo's head at 54 hpf (C, D) and 78 hpf (E–G). Although the VA-L (light blue dotted line) is seen migrating towards the FLS (white dotted lined) on the contralateral side at 54 hpf (C), it is missing from the ablated side (D). Subsequently, the LFL (white dotted line) of the ablated side is short (F) compared to that of the contralateral side (E). In addition, the HA (pink dotted line) is underdeveloped on the ablated side compared to the contralateral side, as it no longer extends towards nor connects to the left AA1 (G).

H Quantitation of the length of the LFL (μm) on the contralateral (control) side and on the ablated side at 78 hpf (n = 16).

I Quantitation of the total number of cells within the LFL on the contralateral (control) side and from the ablated side at 78 hpf (n = 16).

Data information: Error bars represent standard deviation; ****$P < 0.0001$ by unpaired Student's t-test. FLS, facial lymphatic sprout; HA, hypobranchial artery; AA1, first aortic arch; L, left; LDA, lateral dorsal aorta; LFL, lateral facial lymphatic; R, right; VA, ventral aorta lymphangioblast; VA-L, ventral aorta lymphangioblast. Scale bar = 50 μm.

endocardial cells and the primitive myeloid progenitors [37]. During zebrafish development, Cloche/Npas4l functions at the top of the mesodermal-to-angioblast transcriptional cascade [41]. Cloche/Npas4l induces *etv2*, one of the earliest known endothelial and haemangioblast-specific genes, with expression beginning from the 1-somite stage (~10.5 hpf), followed shortly after by *fli1* at the 3-somite stage (~12 h) and subsequently *kdrl* by the 7-somite stage (13–14 hpf) [37,41,45–47]. Similar to early ALPM angioblasts, the VA-A is dependent on *clo/npas4l* activity, but by contrast, the VA-A begins expressing the angioblast-marking transgenes *etv2:EGFP*, *fli1a:nEGFP* and *kdrl:mCherry* approximately 20 h later than the early angioblasts of the head. In addition, *lyve1b:EGFP* expression in the VA-A is observed 10 h later than in the primary veins [32], while the dorsal portion of the VA-A only begins expressing Prox1—indicating differentiation into the VA-L—at least 6 h after lymphatic progenitors are first observed in the CCV and PHS.

Altogether we have four observations supporting the idea that the VA-A is a distinct angioblast population: (i) it expresses angioblast markers (*etv2/fli1/kdrl*), (ii) it is dependent on *clo/npas4l,* (iii) it is able to directly contribute to both the blood and lymphatic vascular networks, and (iv) it migrates as a string of cells rather than sprouting from a lumenised vessel. We propose that by retaining or developing a migratory angioblast-like phenotype, it allows the VA-A the ability to position itself spatiotemporally to contribute towards both facial lymphatic and HA development in an area of the head that is relatively devoid of lymphatic-forming veins. It is possible that other non-venous, lymphatic progenitors in mice may serve the same role; by retaining a migratory phenotype, they

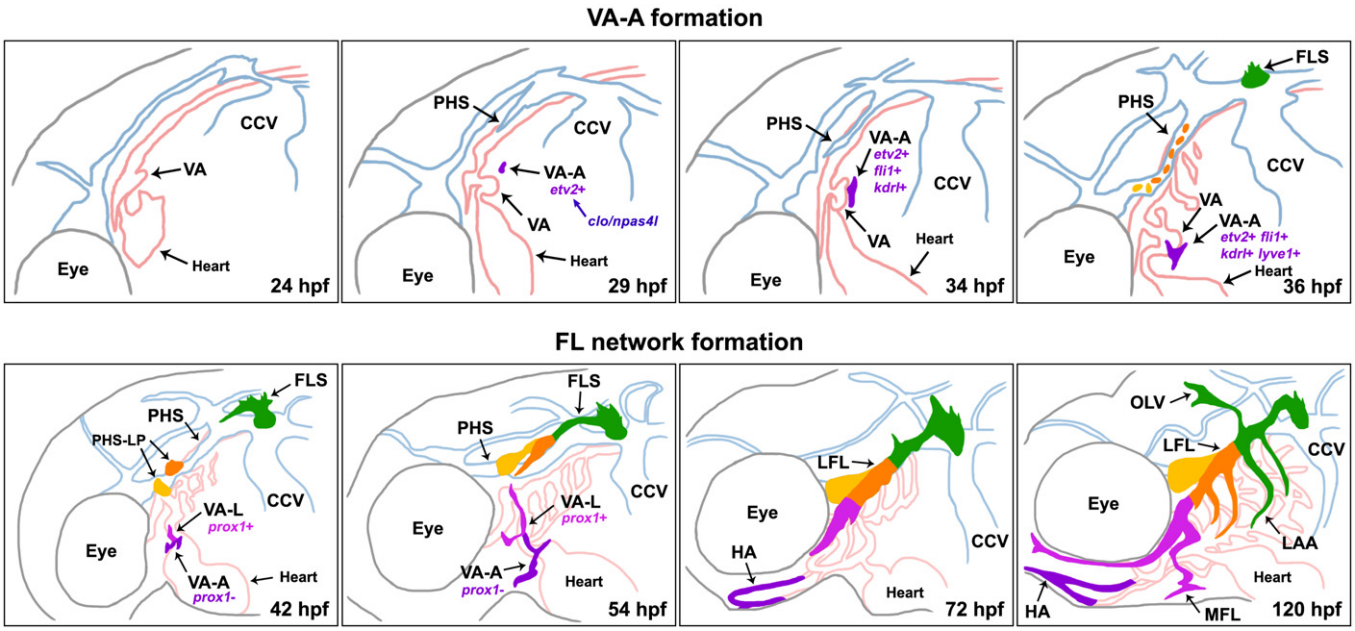

Figure 8. Development of the VA-L and the facial lymphatics.

The VA-A (purple) appears as an isolated, *etv2*-expressing, *clo/npas4l*-dependent angioblast in the anterodorsal yolk sac region at 29 hpf, before migrating ventrally towards the VA and expressing *fli1* and *kdrl* by 34 hpf, and *lyve1b* at 36 hpf. Around this time, facial lymphatic development in the head begins as the FLS (green) arises from the dorsolateral region of the CCV, while lymphatic progenitors become specified in the PHS (orange and yellow cells). At 42 hpf, the dorsal portion of the VA-A differentiates into the VA-L (pink) as it acquires a lymphatic cell fate by turning on Prox1 expression, while the ventral portion of the VA-A remains Prox1-negative (purple). Both the VA-L and the FLS begin migrating dorsally and anteriorly, respectively, towards the PHS, which at this time contains the PHS-LP (orange and yellow) domains. By 54 hpf, the VA-L has reached the FLS tip, which now consists of the PHS-Ls (orange and yellow) that have sprouted from the PHS and fused to the FLS. By 72 hpf, the VA-L has fused to the FLS to form the LFL, while the ventral Prox1-negative VA-A (purple) fuses to its contralateral counterpart and to the first aortic arch to form the HA. At 120 hpf, all components of the facial lymphatic network are present, with the OLV, MFL and LAAs sprouting from the existing LFL. CCV, common cardinal vein; FLS, facial lymphatic sprout; HA, hypobranchial artery; hpf, hours post-fertilisation; LAA, lymphatic branchial arches; LFL, lateral facial lymphatic; MFL, medial facial lymphatic; OLV, otolithic lymphatic vessel; PHS, primary head sinus; VA, ventral aorta; VA-A, ventral aorta angioblast; VA-L, ventral aorta lymphangioblast.

facilitate the formation of lymphatics at sites distant from venous-derived lymph sacs. In support of this, putative non-venous progenitors in the mesentery and dermis arise in areas distal to their respective venous-derived lymph sacs [18,19,22]. Of interest, the zebrafish intestinal lymphatic network develops distinct from the posterior cardinal vein [32], and therefore, it is also possible that non-venous progenitors are also involved in the formation of this lymphatic network.

The mechanisms of facial lymphatic formation are distinct

In this study, we used lineage tracing, cell ablation and live cell imaging to confirm that anatomically distinct veins, the CCV and the PHS, as well as the VA-L, individually contribute lymphangioblasts to the developing facial lymphatic. The distinction between how the zebrafish facial lymphatic develops—involving multiple lymphangioblast sources—compared to the trunk lymphatic network—involving a single source—may be explained by their differing vascular environments. The PCV is a large axial vein that spans the length of the trunk, which allows lymphatic development to occur simultaneously in both the anterior and the posterior of the trunk [23,44]. This is in contrast to the head, where the CCV is found only at its posterior end, with the majority of CCV ECs found in sheets overlaying the yolk sac, rather than within the cranial tissue stroma [33,48]. Thus, rather than relying on multiple sprouts from a single vein as seen in the trunk, the facial lymphatic network forms from the CCV in a polarised manner, growing from the posterior to anterior head and therefore requires additional lymphangioblast populations from both the PHS and the VA-L. Our findings appear to be outwardly similar to two recent descriptions of mammalian lymphatic growth: the dorso-cervical dermal lymphatics, which initially form from the jugular lymph sac but subsequently acquire progenitors from the immature dermal vasculature [22] and the ventral primordial thoracic duct, which arises from the cardinal vein and the superficial venous plexus [5]. We show that these lymphangioblast populations form the facial lymphatic network through sequential cell fusion events in a "relay" mechanism, where the initial CCV-Ls lead FLS migration until they fuse with the PHS-Ls, which then drive lymphatic migration until fusion to cells from the VA-L. Evidence for this mechanism comes from live imaging lymphangioblast migration before and after fusion and is supported by the fact we see little intermingling of cells between photoconverted and non-photoconverted progenitor populations. We also confirmed through cell ablation experiments that the addition of the VA-L is necessary for proper LFL extension under the eye. It remains to be determined what the mechanisms are that coordinate the formation and fusion of these lymphangioblast

populations and whether this "relay" mechanism is observed in other examples of polarised lymphatic vessel growth.

The role of Vegfr3 signalling in facial lymphatic progenitor formation

In mice, PROX1 directly targets and binds the regulatory regions upstream of *Vegfr3* to induce its expression, while *Prox1* transcription and translation are dependent on *Vegfr3* levels, thus forming a positive feedback loop to maintain lymphatic identity within mice LECs [31]. In the zebrafish trunk, loss of *vegfc* and *vegfr3* leads to a pronounced reduction in Prox1 expression in the PCV, while *vegfc* overexpression is sufficient for inducing ectopic expression of Prox1 in venous endothelium [25]. A recent study in zebrafish found that although Erk signalling downstream of Vegfr3 activation is required for trunk lymphatic differentiation and sprouting, it appears dispensable for facial lymphatic specification [29], raising the idea that the role of Vegfr3-signalling in lymphatic specification is context-dependent.

To confirm the role of Vegfr3 signalling in facial lymphatic specification, we used either *ccbe1* morpholino knockdown, which phenocopies the *ccbe1* mutant [28,44] or dominant negative *flt4* (*sFLT4*) mRNA [28,35]. We chose these methods as both approaches are known to completely block facial lymphatic sprouting [28]. Similar to previous studies [29], we found that while either approach blocked facial lymphatic sprouting, it had no effect on lymphatic specification in the CCV. Similarly, the VA-L requires Vegfr3 signalling for migration towards the PHS, yet it is not necessary for initial Prox1 induction in the dorsal VA-L. Finally, we demonstrate that lymphatic PHS-LP domain formation in the PHS is dependent on Vegfr3 signalling; however, it is unclear if this phenotype is the result of a migration/proliferation defect in the PHS-derived lymphatic progenitors or a true inhibition of lymphatic specification. Previous studies have shown that both *vegfc* knockdown and *vegfd* knockdown are required to perturb facial lymphatic development whereas in the trunk, lymphatic development only involves *vegfc* [28,49]. It is possible that the differences in lymphatic specification between the trunk and head are related to this; for example, lymphatic specification in the head may also involve Vegfd-mediated signalling.

In summary, this study reveals the unique mechanisms by which the zebrafish facial lymphatic network is formed. This involves the "relay-like" coalescence of distinct lymphangioblast populations: starting from that of the CCV, followed by the PHS and finally fusing to the VA-L to form the LFL. We show that the VA-L does not sprout from a vein, or indeed any blood vessel, instead arising from a single isolated angioblast cell on the avascular perivitelline space of the anterodorsal yolk sac. We propose that the migratory nature of this progenitor population allows it to contribute to lymphatic development in an area of the head that is relatively devoid of veins, and it provides direct, live imaging-based evidence to support the "dual origin" theory of lymphatic vessel development. Overall, our study further supports the notion that the origin and development of lymphatic vessels is heterogenous between distinct vascular beds [42,43], which has implications for our understanding of both developmental and pathological lymphangiogenesis in organ-specific lymphatic vessels.

Materials and Methods

Zebrafish lines and transgenesis

All zebrafish strains were maintained under standard husbandry conditions and followed protocols approved by the Animal Ethics Committee of the University of Auckland. Adult zebrafish (*Danio rerio*) were maintained in a Tecniplast zebrafish housing facility, controlled by an automated 14–h day/10-h night light cycle with water treated with carbon filters and UV light, and water conditions maintained between 25.5 and 29.5°C, pH 7.2–7.6 and 250–500 μS conductivity. Juvenile and adult fish (> 30 dpf) were fed three times daily on weekdays and once daily on weekends. Larval stage zebrafish (< 30 dpf) were fed on the same schedule. Health checks were done daily to remove sick or dead fish from tanks. All zebrafish used in this study were randomised, and the researchers were not blinded when conducting experiments.

The lines used in this study were *Tg(lyve1b:EGFP)*^{nz150}, *Tg(-lyve1b:DsRed2)*^{nz101} [32], *Tg(kdrl:EGFP)*^{s843} [50], *Tg(kdrl:nlsmCherry)*^{nz49} [51], *TgBAC(flt4:mCitrine)*^{hu7135} [52], *Tg(−0.8flt1:tdTomato)*^{hu5333} [23], *Tg(lyz:DsRed)*^{nz50} [53], *TgBAC(etv2:EGFP)*^{ci1} [37], *TgBAC(etv2:Kaede)*^{ci6} [38], *Tg(fli1a:nEGFP)*^{y7} [54] and *Tg(kdrl:Hsa.HRAS-mCherry)*^{s916} (referred to as *kdrl:mCherry*) [44] and *clo/npas4l*^{s5} [40]. Lines generated in this study are *Tg(lyve1b:Kaede)*^{nz102} and *Tg(kdrl:nlsKaede)*^{nz70}. To make the *lyve1b:Kaede* line, *EGFP* was excised from the original pt2k/*lyve1b:EGFP* Tol2 construct [32] using BamHI and ClaI. *Kaede* was then PCR amplified using cDNA from *Tg(mpeg1:Gal4)*^{gl24};*Tg(UAS:Kaede)*^{s1999t} embryos [55], using primers flanked by BamHI (5′) and ClaI (3′) restriction enzyme sites, and directionally cloned into the EGFP site of the pT2KXIGΔin vector containing the *lyve1b* promoter. To make the *kdrl:nlsKaede* line, the approximately 6.5 kb *kdrl* promoter fragment was liberated from pCRII-TOPO:*kdrl* (a gift from Didier Stainier) [50], using BamHI and EcoRV, and directionally cloned into BamHI/SacI(blunted)-linearised p5E-MCS [56] to generate p5E:*-6.5kdrl*. Using Gateway technology (Invitrogen), a two-fragment LR recombination reaction was performed using the p5E:*-6.5kdrl*, pME:*nlsKaede* (kindly provided by P. Currie and P. Nguyen) and pTol-DestR4-R2pA [56] fragments to make the *kdrl:nlsKaede* Tol2 construct. Stable transgenic lines were generated as previously described [53].

Photoconversion

lyve1b:Kaede (36–72 hpf), *kdrl:nlsKaede* (24–33 hpf) and *etv2:Kaede* (24–33 hpf) embryos were mounted as previously described [57] and photoconverted using an Olympus FV1000 confocal microscope equipped with a diode-pumped 405 nm laser. Specific Kaede-positive structures or populations were converted by highlighting a region of interest using FluoView 3.0 (Olympus) software and exposing them to 405 nm laser light using a SIM Scanner for 5–10 s. Embryos were imaged immediately after photoconversion with a Nikon D-Eclipse C1 confocal microscope, followed by rescue from the agarose and then individual sorting into numbered wells of tissue culture plates for later identification. Each larva was subsequently imaged again 12–48 h post-conversion. During post-processing, representative images were falsely coloured in purple using Volocity 6.3 software

(Improvision/PerkinElmer Life and Analytical Sciences) to highlight the overlap between (Kaede) green and (photoconverted) red pixels.

Morpholino and mRNA injections

Morpholino injections were performed on *lyve1b:EGFP*, *etv2:EGFP* or *etv2:EGFP;kdrl:nlsmCherry* embryos as previously described [58]. Embryos between the 1 and 4-cell stage were injected either with 5 ng standard control morpholino (Gene Tools), 10 ng *ccbe1* morpholino [44], 2 ng *csf3r* and 5 ng *pu.1* morpholino [36] or 6.4 ng ATG and 1.8 ng splice-blocking *clo/npas4l* morpholinos [41]. The *ccbe1* morpholino has previously been shown to phenocopy the *fof* mutant [44], the combination of *csf3r* and *pu.1* morpholinos has previously been shown to broadly inhibit myelopoiesis [36], and the combination of two distinct *clo/npas4l* morpholinos, each at a suboptimal dose, has previously been shown to phenocopy the *cloche* mutant [41]. The pCS2$^+$/*sFLT4* construct [27] and protocol for synthesis and injection of 200 pg *sFLT4* mRNA into single-cell embryos have been previously described [28].

Ablations

Cell ablations were performed on *etv2:EGFP;kdrl:nlsmCherry* embryos at 30 hpf using an Olympus FV1000 confocal microscope equipped with a diode-pumped 405 nm laser. The *etv2*-expressing VA-A on the left lateral side of the zebrafish head was highlighted using FluoView 3.0 (Olympus) software and exposed to 405 nm laser light at maximum intensity using a SIM Scanner and with an open pinhole for 10–15 min. Embryos were also imaged immediately before and after ablation using the Olympus FV1000 confocal microscope. Ablated embryos were reimaged 3 h following ablation to ensure the cells had been fully ablated. Each larva was subsequently imaged again at 48 and 78 hpf using a Nikon D-Eclipse C1 confocal microscope.

Immunohistochemistry

Prox1 immunofluorescence staining was performed as described [25], with DAPI (1:400, Invitrogen) added during the secondary antibody incubation step for cell count quantitation. Antibodies used in this study were chicken anti-GFP (1:400, Abcam, #ab13970), rabbit anti-PROX1 (1:500, AngioBio Co, #11-002P) and anti-rabbit IgG-HRP (1:1,000, Cell Signaling, #7074). Superficial, non-specific, background staining in Prox1 immunofluorescence images was removed during post-processing using Photoshop CC 2015 (Adobe).

Confocal imaging

Live and fixed embryos were mounted laterally or ventrolaterally and imaged as previously described [57] with a Nikon D-Eclipse C1 confocal microscope and/or an Olympus FV1000 confocal microscope for either still or time-lapse microscopy. *Z*-stacks of still images were acquired at 5 μm increments with a 20× objective or 4 μm increments with a 60× objective. For time-lapse microscopy, *z*-stacks were taken at 10-min intervals. Images were processed using Fiji [59], Photoshop CC 2015 (Adobe) and Volocity 6.3 image analysis software (Improvision/PerkinElmer Life and Analytical Sciences).

Image analysis and statistics

All quantitative analyses were performed using Volocity 6.3 software. Endothelial nuclei were identified using DAPI and anti-GFP in fixed *Tg(lyve1b:EGFP)* larvae. Lymphatic precursors or lymphangioblasts were identified using DAPI, anti-GFP and anti-Prox1 in fixed *Tg(lyve1b:EGFP)* larvae. Lymphatic precursors that co-expressed DAPI, GFP and Prox1 within the FLS, PHS and VA-L were manually counted through the complete confocal *z*-stack at 36 and 42 hpf. In morpholino and mRNA injection studies, this was expressed as a percentage of the total number of GFP and DAPI-positive endothelial nuclei within each vessel. Using time-lapse confocal images, the total number of lymphangioblast nuclei [expressing *Tg(lyve1b:EGFP)* and *Tg(kdrl:nlsmCherry)*] within the developing FLS was also manually counted across the complete confocal *z*-stack at 1.5-h intervals from 43.5 to 58.5 hpf. Lymphangioblast velocity was calculated by tracking and measuring the total distance (in μm) a single tip cell travelled over 3–3.5 h (180–210 min) prior to fusing with the next lymphangioblast population, followed by the length travelled by the same cell 3–3.5 h post-fusion. Statistical analyses were performed using Prism 7.0 software (GraphPad Software). Significance was determined by unpaired Student's *t*-test or one-way ANOVA, and normality of the data sets was confirmed using the Shapiro–Wilk normality test.

Expanded View for this article is available online.

Acknowledgements
We thank Mr Alhad Mahagaonkar for managing the fish facility and the Biomedical Imaging Research Unit, University of Auckland, for assistance in microscopy and cell ablation. We also thank the Sumanas laboratory for providing the *etv2:EGFP* and *etv2:Kaede* lines. Work in this study was supported by a Health Research Council of New Zealand project grant (14/105) awarded to P.S.C and J.W.A and a Royal Society of New Zealand Marsden Project Grant (UOA1602) awarded to J.W.A. T.C.Y.E was supported by the University of Auckland Doctoral Scholarship and the School of Medical Sciences Performance-based Research Fund Publication Assistance Bursary awarded by the University of Auckland. Y.P. and S.S.-M. were supported by the CiM Cluster of Excellence (EXC 1003-CiM), and CRC 1348 and SCHU1228/3-1 from the DFG.

Author contributions
Conceptualisation: TCYE, KSO, JWA; Methodology: TCYE, KSO, CJH, BMH, JWA; Investigation: TCYE, JPM, KSO, YP, WC, JWA; Writing and Review: TCYE, JWA; Funding Acquisition: KEC, PSC, SS-M, JWA.

Conflict of interest
The authors declare that they have no conflict of interest.

References

1. Hong Y, Harvey N, Noh Y, Schacht V, Hirakawa S, Detmar M, Oliver G (2002) Prox1 is a master control gene in the program specifying lymphatic endothelial cell fate. *Dev Dyn* 225: 351 – 357

2. Wigle JT, Oliver G (1999) Prox1 function is required for the development of the murine lymphatic system. *Cell* 98: 769 – 778
3. Karkkainen MJ, Haiko P, Sainio K, Partanen J, Taipale J, Petrova TV, Jeltsch M, Jackson DG, Talikka M, Rauvala H (2004) Vascular endothelial growth factor C is required for sprouting of the first lymphatic vessels from embryonic veins. *Nat Immunol* 5: 74 – 80
4. Zhang L, Zhou F, Han W, Shen B, Luo J, Shibuya M, He Y (2010) VEGFR-3 ligand-binding and kinase activity are required for lymphangiogenesis but not for angiogenesis. *Cell Res* 20: 1319 – 1331
5. Hägerling R, Pollmann C, Andreas M, Schmidt C, Nurmi H, Adams RH, Alitalo K, Andresen V, Schulte-Merker S, Kiefer F (2013) A novel multistep mechanism for initial lymphangiogenesis in mouse embryos based on ultramicroscopy. *EMBO J* 32: 629 – 644
6. François M, Short K, Secker GA, Combes A, Schwarz Q, Davidson T, Smyth I, Hong Y, Harvey NL, Koopman P (2012) Segmental territories along the cardinal veins generate lymph sacs via a ballooning mechanism during embryonic lymphangiogenesis in mice. *Dev Biol* 364: 89 – 98
7. Yang Y, García-Verdugo JM, Soriano-Navarro M, Srinivasan RS, Scallan JP, Singh MK, Epstein JA, Oliver G (2012) Lymphatic endothelial progenitors bud from the cardinal vein and intersomitic vessels in mammalian embryos. *Blood* 120: 2340 – 2348
8. Sabin FR (1902) On the origin of the lymphatic system from the veins and the development of the lymph hearts and thoracic duct in the pig. *Am J Anat* 1: 367 – 389
9. Huntington GS (1908) Symposium on the development and structure of the lymphatic system. II. The genetic in erpretation of the development of the mammalian lymphatic system. *Anat Rec* 2: 19 – 45
10. Huntington GS, McClure CF (1910) The anatomy and development of the jugular lymph sacs in the domestic cat (Felis domestica). *Am J Anat* 10: 177 – 312
11. Yaniv K, Isogai S, Castranova D, Dye L, Hitomi J, Weinstein BM (2006) Live imaging of lymphatic development in the zebrafish. *Nat Med* 12: 711 – 716
12. Srinivasan RS, Dillard ME, Lagutin OV, Lin FJ, Tsai S, Tsai MJ, Samokhvalov IM, Oliver G (2007) Lineage tracing demonstrates the venous origin of the mammalian lymphatic vasculature. *Genes Dev* 21: 2422 – 2432
13. der Jagt Van, Raymond Ervin (1932) Memoirs: the origin and development of the anterior lymph-sacs in the sea-turtle (Thalassochelys caretta). *J Cell Sci* 2: 151 – 163
14. Wilting J, Aref Y, Huang R, Tomarev SI, Schweigerer L, Christ B, Valasek P, Papoutsi M (2006) Dual origin of avian lymphatics. *Dev Biol* 292: 165 – 173
15. Wilting J, Papoutsi M, Othman-Hassan K, Rodriguez-Niedenführ M, Pröls F, Tomarev SI, Eichmann A (2001) Development of the avian lymphatic system. *Microsc Res Tech* 55: 81 – 91
16. Ny A, Koch M, Schneider M, Neven E, Tong RT, Maity S, Fischer C, Plaisance S, Lambrechts D, Héligon C (2005) A genetic *Xenopus laevis* tadpole model to study lymphangiogenesis. *Nat Med* 11: 998 – 1004
17. Klotz L, Norman S, Vieira JM, Masters M, Rohling M, Dubé KN, Bollini S, Matsuzaki F, Carr CA, Riley PR (2015) Cardiac lymphatics are heterogeneous in origin and respond to injury. *Nature* 522: 62 – 67
18. Stanczuk L, Martinez-Corral I, Ulvmar MH, Zhang Y, Laviña B, Fruttiger M, Adams RH, Saur D, Betsholtz C, Ortega S (2015) cKit lineage hemogenic endothelium-derived cells contribute to mesenteric lymphatic vessels. *Cell Rep* 10: 1708 – 1721
19. Martinez-Corral I, Ulvmar M, Stanczuk L, Tatin F, Kizhatil K, John SW, Alitalo K, Ortega S, Makinen T (2015) Non-venous origin of dermal lymphatic vasculature. *Circ Res* 116: 1649 – 1654
20. Ulvmar MH, Martinez-Corral I, Stanczuk L, Mäkinen T (2016) Pdgfrb-Cre targets lymphatic endothelial cells of both venous and non-venous origins. *Genesis* 54: 350 – 358
21. Heffner CS, Pratt CH, Babiuk RP, Sharma Y, Rockwood SF, Donahue LR, Eppig JT, Murray SA (2012) Supporting conditional mouse mutagenesis with a comprehensive cre characterization resource. *Nat Commun* 3: 1218
22. Pichol-Thievend C, Betterman KL, Liu X, Ma W, Skoczylas R, Lesieur E, Bos FL, Schulte D, Schulte-Merker S, Hogan BM *et al* (2018) A blood capillary plexus-derived population of progenitor cells contributes to genesis of the dermal lymphatic vasculature during embryonic development. *Development* 145: dev160184
23. Bussmann J, Bos FL, Urasaki A, Kawakami K, Duckers HJ, Schulte-Merker S (2010) Arteries provide essential guidance cues for lymphatic endothelial cells in the zebrafish trunk. *Development* 137: 2653 – 2657
24. Nicenboim J, Malkinson G, Lupo T, Asaf L, Sela Y, Mayseless O, Gibbs-Bar L, Senderovich N, Hashimshony T, Shin M (2015) Lymphatic vessels arise from specialized angioblasts within a venous niche. *Nature* 522: 56 – 61
25. Koltowska K, Lagendijk AK, Pichol-Thievend C, Fischer JC, Francois M, Ober EA, Yap AS, Hogan BM (2015) Vegfc regulates bipotential precursor division and Prox1 expression to promote lymphatic identity in zebrafish. *Cell Rep* 13: 1828 – 1841
26. Küchler AM, Gjini E, Peterson-Maduro J, Cancilla B, Wolburg H, Schulte-Merker S (2006) Development of the zebrafish lymphatic system requires *vegfc* signaling. *Curr Biol* 16: 1244 – 1248
27. Hogan BM, Herpers R, Witte M, Helotera H, Alitalo K, Duckers HJ, Schulte-Merker S (2009) Vegfc/Flt4 signalling is suppressed by Dll4 in developing zebrafish intersegmental arteries. *Development* 136: 4001 – 4009
28. Astin JW, Haggerty MJ, Okuda KS, Le Guen L, Misa JP, Tromp A, Hogan BM, Crosier KE, Crosier PS (2014) Vegfd can compensate for loss of Vegfc in zebrafish facial lymphatic sprouting. *Development* 141: 2680 – 2690
29. Shin M, Male I, Beane TJ, Villefranc JA, Kok FO, Zhu LJ, Lawson ND (2016) Vegfc acts through ERK to induce sprouting and differentiation of trunk lymphatic progenitors. *Development* 143: 3785 – 3795
30. Bowles J, Secker G, Nguyen C, Kazenwadel J, Truong V, Frampton E, Curtis C, Skoczylas R, Davidson T, Miura N (2014) Control of retinoid levels by CYP26B1 is important for lymphatic vascular development in the mouse embryo. *Dev Biol* 386: 25 – 33
31. Srinivasan RS, Escobedo N, Yang Y, Interiano A, Dillard ME, Finkelstein D, Mukatira S, Gil HJ, Nurmi H, Alitalo K *et al* (2014) The Prox1-Vegfr3 feedback loop maintains the identity and the number of lymphatic endothelial cell progenitors. *Genes Dev* 28: 2175 – 2187
32. Okuda KS, Astin JW, Misa JP, Flores MV, Crosier KE, Crosier PS (2012) Lyve1 expression reveals novel lymphatic vessels and new mechanisms for lymphatic vessel development in zebrafish. *Development* 139: 2381 – 2391
33. Isogai S, Horiguchi M, Weinstein BM (2001) The vascular anatomy of the developing zebrafish: an atlas of embryonic and early larval development. *Dev Biol* 230: 278 – 301
34. Crucke J, Huysseune A (2013) Unravelling the blood supply to the zebrafish pharyngeal jaws and teeth. *J Anat* 223: 399 – 409
35. Ober EA, Olofsson B, Makinen T, Jin SW, Shoji W, Koh GY, Alitalo K, Stainier DY (2004) Vegfc is required for vascular development and endoderm morphogenesis in zebrafish. *EMBO Rep* 5: 78 – 84
36. Pase L, Layton JE, Wittmann C, Ellett F, Nowell CJ, Reyes-Aldasoro CC, Varma S, Rogers KL, Hall CJ, Keightley MC (2012) Neutrophil-delivered

myeloperoxidase dampens the hydrogen peroxide burst after tissue wounding in zebrafish. *Curr Biol* 22: 1818 – 1824

37. Proulx K, Lu A, Sumanas S (2010) Cranial vasculature in zebrafish forms by angioblast cluster-derived angiogenesis. *Dev Biol* 348: 34 – 46
38. Kohli V, Schumacher JA, Desai SP, Rehn K, Sumanas S (2013) Arterial and venous progenitors of the major axial vessels originate at distinct locations. *Dev Cell* 25: 196 – 206
39. Pham VN, Lawson ND, Mugford JW, Dye L, Castranova D, Lo B, Weinstein BM (2007) Combinatorial function of ETS transcription factors in the developing vasculature. *Dev Biol* 303: 772 – 783
40. Stainier DY, Weinstein BM, Detrich HW III, Zon LI, Fishman MC (1995) Cloche, an early acting zebrafish gene, is required by both the endothelial and hematopoietic lineages. *Development* 121: 3141 – 3150
41. Reischauer S, Stone OA, Villasenor A, Chi N, Jin S, Martin M, Lee MT, Fukuda N, Marass M, Witty A (2016) Cloche is a bHLH-PAS transcription factor that drives haemato-vascular specification. *Nature* 535: 294
42. Potente M, Mäkinen T (2017) Vascular heterogeneity and specialization in development and disease. *Nat Rev Mol Cell Biol* 18: 477
43. Wong B, Zecchin A, García-Caballero M, Carmeliet P (2018) Emerging concepts in organ-specific lymphatic vessels and metabolic regulation of lymphatic development. *Dev Cell* 45: 289 – 301
44. Hogan BM, Bos FL, Bussmann J, Witte M, Chi NC, Duckers HJ, Schulte-Merker S (2009) *ccbe1* is required for embryonic lymphangiogenesis and venous sprouting. *Nat Genet* 41: 396 – 398
45. Thompson MA, Ransom DG, Pratt SJ, MacLennan H, Kieran MW, Detrich HW III, Vail B, Huber TL, Paw B, Brownlie AJ (1998) The cloche and spadetail genes differentially affect hematopoiesis and vasculogenesis. *Dev Biol* 197: 248 – 269
46. Liao W, Bisgrove BW, Sawyer H, Hug B, Bell B, Peters K, Grunwald DJ, Stainier DY (1997) The zebrafish gene cloche acts upstream of a flk-1 homologue to regulate endothelial cell differentiation. *Development* 124: 381 – 389
47. Sumanas S, Gomez G, Zhao Y, Park C, Choi K, Lin S (2008) Interplay among Etsrp/ER71, Scl, and Alk8 signaling controls endothelial and myeloid cell formation. *Blood* 111: 4500 – 4510
48. Helker CS, Schuermann A, Karpanen T, Zeuschner D, Belting HG, Affolter M, Schulte-Merker S, Herzog W (2013) The zebrafish common cardinal veins develop by a novel mechanism: lumen ensheathment. *Development* 140: 2776 – 2786
49. Bower NI, Vogrin AJ, Le Guen L, Chen H, Stacker SA, Achen MG, Hogan BM (2017) Vegfd modulates both angiogenesis and lymphangiogenesis during zebrafish embryonic development. *Development* 144: 507 – 518
50. Jin SW, Beis D, Mitchell T, Chen JN, Stainier DY (2005) Cellular and molecular analyses of vascular tube and lumen formation in zebrafish. *Development* 132: 5199 – 5209
51. Lam EY, Hall CJ, Crosier PS, Crosier KE, Flores MV (2010) Live imaging of Runx1 expression in the dorsal aorta tracks the emergence of blood progenitors from endothelial cells. *Blood* 116: 909 – 914
52. van Impel A, Zhao Z, Hermkens DM, Roukens MG, Fischer JC, Peterson-Maduro J, Duckers H, Ober EA, Ingham PW, Schulte-Merker S (2014) Divergence of zebrafish and mouse lymphatic cell fate specification pathways. *Development* 141: 1228 – 1238
53. Hall CJ, Flores MV, Storm T, Crosier KE, Crosier PS (2007) The zebrafish lysozyme C promoter drives myeloid-specific expression in transgenic fish. *BMC Dev Biol* 7: 42
54. Roman BL, Pham VN, Lawson ND, Kulik M, Childs S, Lekven AC, Garrity DM, Moon RT, Fishman MC, Lechleider RJ *et al* (2002) Disruption of acvrl1 increases endothelial cell number in zebrafish cranial vessels. *Development* 129: 3009 – 3019
55. Hall CJ, Boyle RH, Astin JW, Flores MV, Oehlers SH, Sanderson LE, Ellett F, Lieschke GJ, Crosier KE, Crosier PS (2013) Immunoresponsive gene 1 augments bactericidal activity of macrophage-lineage cells by regulating β-oxidation-dependent mitochondrial ROS production. *Cell Metab* 18: 265 – 278
56. Kwan KM, Fujimoto E, Grabher C, Mangum BD, Hardy ME, Campbell DS, Parant JM, Yost HJ, Kanki JP, Chien C (2007) The Tol2kit: a multisite gateway-based construction kit for Tol2 transposon transgenesis constructs. *Dev Dyn* 236: 3088 – 3099
57. Hall CJ, Flores MV, Crosier KE, Crosier PS (2009) Live cell imaging of zebrafish leukocytes. *Methods Mol Biol* 546: 255 – 271
58. Nasevicius A, Ekker SC (2000) Effective targeted gene 'knockdown'in zebrafish. *Nat Genet* 26: 216
59. Schindelin J, Arganda-Carreras I, Frise E, Kaynig V, Longair M, Pietzsch T, Preibisch S, Rueden C, Saalfeld S, Schmid B (2012) Fiji: an open-source platform for biological-image analysis. *Nat Methods* 9: 676 – 682